

Study of novel properties of graphene-ZnO heterojunction interface using density functional theory

H.D. Etea, K.N. Nigussa*

Department of Physics, Addis Ababa University, P.O. Box 1176, Addis Ababa, Ethiopia

Abstract

Studies of the structural, electronic, and optical characteristics of the interfaces between graphene and ZnO polar surfaces is carried out using first-principles simulations. At the interface, a strong van der Waals force is present, and because of the different work functions of graphene and ZnO, charge transfer takes place. Graphene's superior conductivity is not impacted by its interaction with ZnO, since its Dirac point is unaffected despite its adsorption on ZnO. In hybrid systems, excited electrons with energies between 0 and 3 eV (above Fermi energy) are primarily accumulated on graphene. The calculations offer a theoretical justification for the successful operation of graphene / ZnO hybrid materials as photocatalysts and solar cells. ZnO semiconductor is found to be a suitable material with modest band gap, (~ 3 eV), having high transparency in visible region and a high optical conductivity.

Keywords: Zinc oxide, Graphene, Density functional theory, Heterojunction.

1. Introduction

The ultimate spintronics device can be thought of as the interface between materials since it allows for new design possibilities and physical features that are not possible in the individual bulk materials [1]. Rashba-Edelstein spin-to-charge conversion and spin-momentum locking at the surface of topological insulators are two emerging interfacial phenomena caused by spin-orbit coupling (SOC). Interfaces naturally break spatial inversion symmetry, which causes an electronic band Rashba SO splitting that is often higher than in bulk. In particular, SO effects at oxide interfaces are crucial for low-power spintronics applications due to the expected long carrier lifetime and high Rashba coefficient [2]. Carbon-based nanomaterials are prime candidates for spin-based devices, due to their long spin coherence length (up to 10^4 ps) and high Fermi velocity [3]. Since the successful exploitation of single-layer graphene in 2004 by Geim and his co-workers [4], the investigations on the interaction of graphene and other nanomaterials have become a growing trend due to the extraordinary properties of graphene, such as the Dirac electrons near the K point, room-temperature quantum Hall effect, and high mobility of carrier electrons [5]. Research on the interaction of graphene with BN [6], SiC [7], metals [8], or metal oxides [9] has been done both experimentally and computationally thus far. The study of graphene-based interfaces is of great importance in materials production [10], device fabrication [11], and electrical measurement [12], because the contact of other materials with graphene may modify the physical and chemical properties of graphene and then influence its performance in devices.

In recent years, zinc oxide (ZnO) has attracted great attention in the field of nanodevices as an important semiconductor because of its unique optical, electronic, and magnetic properties, including large excitation binding energy (60 meV), wide band gap (3.4 eV), and unique piezoelectric properties [13]. A review of the literature reveals that the wide band gap, > 3 eV, ZnO semiconductor is a suitable material with great transparency in the visible region and good optical conductivity. Some of ZnO properties are improved when it is synthesized in the form of nanosized material and, for this reason, a wide range of ZnO nanostructures have been lately obtained [14] such as nanohelices, nanobows, nanorings, nanowires, and nanocages, which are promising candidates for gas sensors, solar cells, field

*Corresponding author: kenate.nemera@aau.edu.et (K.N. Nigussa)

effect transistors, photocatalysts, and so on [15].

These materials display unique features such as greater photovoltaic properties than graphene or bulk ZnO alone in solar cells [16] and photocatalysts [17]. Despite the varied morphologies of graphene hybridizations with ZnO nanoparticles and vertical nanostructures, it is generally accepted that graphene's high specific surface area facilitates the loading of dyes in photocatalysis, and that charge transfer processes that involve charge-hole separation and transfer from graphene to ZnO are facilitated by graphene's higher conductivity. With significant experimental advancement, a computational investigation of graphene-ZnO hybrid systems has also been carried out [18]. In this work, the structural, interaction, and electronic properties of graphene-ZnO hybrid systems were investigated through density functional theory (DFT) computations to better understand the experimental results and hidden mechanisms.

The paper is organized as follows. In the next section (sec. 2), a detail account of the computational method is presented. Results and discussion are presented in section 3, with the conclusion being presented in section 4.

2. Computational Methods

All calculations in this work were carried out using the GPAW code, where the detail of the capabilities is described in a literature [19]. The exchange-correlation energy of the interacting electrons is expressed using the frozen-core full potential projector augmented wave (PAW) approach [20] and the Perdew-Burke-Ernzerhof (PBE) form [21]. The electronic ground state was determined using the plane waves basis with a cut-off energy of 400 eV and the conjugate gradient algorithm, with the convergence threshold set at 5×10^{-4} eV for energy and 0.01 eV/Å for force. The Brillouin zone integrations were carried out using Monkhorst-Pack grids [22]. We used k-point meshes of $6 \times 6 \times 6$ for a wurtzite ZnO primitive cell, $6 \times 6 \times 1$ for a graphene primitive cell, ZnO (001) polar surfaces, and the supercells of the interface. A dipole correction [23] was applied to make the computations converge more quickly and to eliminate the artificial electrostatic field between periodic supercells.

The electron wave-function is approximated using the implementation of the projector augmented wave (PAW) method and as expanded in a plane wave basis set [24] having a band, a k-points, and a reciprocal lattice vector grid indices. The electron energy eigenvalues are obtained by applying Schrödinger equation and solving self-consistently via the Kohn-Sham scheme [25]. The interactions of the valence electrons with the core electrons and nuclei is treated within a projector augmented wave (paw) data sets [26, 27]. The number of valence electrons considered for each element within the paw data sets is Zn ($3d^{10}4s^2$), O ($2s^22p^4$), C ($2s^22p^4$). Geometry relaxations are carried out using BFGS minimizer [28], where optimization of the atomic forces and the unit cell stresses is done within the concepts of the Hellmann-Feynman forces and stresses [29, 30] calculated on the Born-Oppenheimer (BO) surface [31]. The exchange-correlation energies are approximated within the generalized gradient approximation of PBE [32]. The strongly correlated nature of d electrons of Zn were treated using Hubbard-like model which is introduced into the Gpaw code according to [33, 34], where $U-J=9.5$ eV.

Spin polarized calculation is applied where a magnetic moment on each atom is allowed to relax to optimum value. Density of states (DOS) is calculated as a population of states available for occupation at a given energy.

Equilibrium volumes and bulk modulus are calculated using Murnaghan equation of state [35]. Cohesive energy is calculated as the energy required to break atoms of the solid into a constituent isolated atoms, as described elsewhere [36]. In the models of the interface, vdW interactions are expected to be significant and thus the DFT-D2 method of Grimme [37], which is successful for graphene/SiC interface structures [38] was adopted in this work. The total energy (E_{total}) is represented as:

$$E_{total} = E_{KS-DFT} + E_{vdW} \quad (1)$$

where E_{KS-DFT} is the conventional Kohn-Sham DFT energy and E_{vdW} is the dispersion correction. Note that Vanin et al [39] reported that the vdW-DF method proposed by Dion et al [40] failed to reproduce the experimental observations of the metal-graphene interface. When doing a spin polarized computation, a magnetic moment on each atom is allowed to relax to its optimum value.

In this work, the ZnO wurtzite structure with unit cells of 6 atoms in $P6_{3mc}$ is taken into consideration. After these frameworks were set up, literature resources [41], were carefully followed. The number of states that are occupied at a given level of energy is used to compute the density of states (DOS). Tetrahedron approach was used to do Brillouin zone integration, and it has been shown to be effective, particularly for calculations of excited states and dielectric functions [42].

The optical response property is analysed from dielectric function, which is given as

$$\varepsilon(\omega) = \varepsilon_1(\omega) + i\varepsilon_2(\omega) \quad (2)$$

The imaginary part $\varepsilon_2(\omega)$ is calculated from the density matrix of the electronic structure [43] according to the implementations by the group of G. Kresse [44, 45], & given by

$$\varepsilon_2(\omega) = \frac{8\pi^2 e^2 \hbar^2}{\Omega \omega^2 m_e^2} \sum_{\mathbf{k}, \mathbf{v}, \mathbf{c}} w_{\mathbf{k}} |\langle \psi_{\mathbf{k}}^c | \mathbf{u} \cdot \mathbf{r} | \psi_{\mathbf{k}}^v \rangle|^2 \delta(E_{\mathbf{k}}^c - E_{\mathbf{k}}^v - \hbar\omega), \quad (3)$$

where e is the electronic charge, and $\psi_{\mathbf{k}}^c$ and $\psi_{\mathbf{k}}^v$ are the conduction band (CB) and valence band (VB) wave functions at \mathbf{k} , respectively, $\hbar\omega$ is the energy of the incident photon, $\mathbf{u} \cdot \mathbf{r}$ is the momentum operator, $w_{\mathbf{k}}$ is a joint density of states, & Ω is volume of the primitive cell.

The Real part $\varepsilon_1(\omega)$ of the dielectric function can be found from the Kramer-Kronig equation [46].

$$\varepsilon_1(\omega) = 1 + \frac{2}{\pi} P \int_0^\infty \frac{\omega' \varepsilon_2(\omega')}{\omega'^2 - \omega^2} d\omega' \quad (4)$$

where, P stands for the principal value of the integral. The optical absorption coefficient was obtained by using Eq. (5)

$$\alpha = \sqrt{2} \frac{\omega}{c} \sqrt{\sqrt{\varepsilon_1^2(\omega) + \varepsilon_2^2(\omega)} - \varepsilon_1(\omega)} \quad (5)$$

where ω is photon frequency, and c is speed of light. ε_1 & ε_2 are frequency dependent real and imaginary parts of dielectric function as stated in Eq. (5). From dielectric function, all the other optical properties such as, reflectivity R , refractive index n , & extinction coefficient κ is also obtained [47–49]. Refractive index is calculated by

$$n(\omega) = \frac{1}{\sqrt{2}} \sqrt{\sqrt{\varepsilon_1^2(\omega) + \varepsilon_2^2(\omega)} + \varepsilon_1(\omega)} \quad (6)$$

while reflectivity $R(\omega)$, & energy loss function $\iota(\omega)$ is calculated as

$$R(\omega) = \left| \frac{\sqrt{\varepsilon(\omega)} - 1}{\sqrt{\varepsilon(\omega)} + 1} \right|^2 \quad (7)$$

and

$$\iota(\omega) = \frac{\varepsilon_2(\omega)}{\left[\varepsilon_1^2(\omega) + \varepsilon_2^2(\omega) \right]}, \quad (8)$$

respectively.

3. Results and Discussion

Since ZnO exhibits various structures, making duly comparison between structures on the relative stabilities and the conditions is necessary while studies of heterojunction design is considered. Some of the bulk properties of ZnO crystal is studies by calculating Cohesive energies, formation energies, and bulk modulus, described as follows. The cohesive and formation energies are calculated according to formula given our previous work [36]. Accordingly, as shown in Table 1, the cohesive energy of bulk ZnO structure in WZ (B_4) > ZB (B_3) > RS (B_1). That means ZnO is more stable in wurtzite (WZ) structure, followed by zincblende (BZ) structure and is least stable for rocksalt (RS) structure. From energy per atom calculation, WZ (B_4) > ZB (B_3) > RS (B_1). Furthermore, the degree of covalency is shown from charge values to be according to WZ (B_4) > ZB (B_3) > RS (B_1). Positive values of E_{coh} in means exothermic process while negative values mean endothermic process.

Table 1: Cohesive energy [eV/atom], formation energy [eV], band gap [eV], bulk modulus [GPa] and lattice constant [\AA] of bulk ZnO.

Quantity	Source	Structure		
		WZ (B_4)	ZB (B_3)	RS (B_1)
E_{coh}	This work	2.84	1.10	0.94
	Expt value	1.93 [50]	0.96 [50]	0.93 [50]
E_f	This work	-1.25	2.70	2.86
	Expt value	-3.70 [50]	-	-
Bulk modulus	This work	137.6	131.3	169.9
	Expt value	142.4 [51]	-	-
Band gap	This work	3.23	3.18	3.99
	Expt value			-
Lattice const (a)	This work	3.4	4.4	4.1
	Expt value	3.25	-	-
Lattice const (c)	This work	5.14	-	-
	Expt value	5.2	-	-
Energy per atom	This work	-3.32	-1.58	-1.41
	Expt value	-	-	-
$\Delta Q[e]$ on Zn	This work	+0.23	+0.25	+0.41
	Expt value	-	-	-
$\Delta Q[e]$ on O	This work	-0.23	-0.25	-0.41
	Expt value	-	-	-

In terms of formation energy in reference to Table 1, thus, E_f of bulk ZnO structure in WZ (B_4) < ZB (B_3) < RS (B_1). This means ZnO alloy is more favorable to be formed in wurtzite (B_4) structure. Furthermore, based on the bulk modulus values of ZnO structures presented in Table 1, WZ (B_4) > ZB (B_3) > RS (B_1). This means, ZnO alloy is more resistant to extreme pressure conditions in wurtzite structure. Negative values of E_f in means exothermic process while positive values mean endothermic process. From a curve fits according to Murnaghan [?] approach, to an energy versus volume calculation data, the bulk modulus, minimum volume and minimum energy values are obtained, as shown in the Table 1.

Accordingly, the output parameters of lattice constants (a), (c), and bulk modulus (B) for B_4 structure in this work are 3.4 \AA , 5.14 \AA , and 137.59 GPa respectively. But the experimental results of lattice constants (a), (c), and bulk modulus (B) are 3.25 \AA [52], 5.2 \AA [52], and 142.4 GPa [51], respectively. The results show that even though there is small differences in between the computational and the experimental results, the two are essentially in agreement with each other. This gives us a confidence on the predicted properties of heterojunction structures considered in this study. The surface energy σ [eV/ \AA^2] is defined as

$$\sigma = \frac{1}{2A} \left(E_{\text{slab}} - \frac{N_{\text{slab}}}{N_{\text{bulk}}} E_{\text{bulk}} \right) \quad (9)$$

where E_{slab} denotes the total energy of a slab unit cell, N_{slab} , means number of atoms in the slab unit cell, N_{bulk} means number of atoms in the bulk unit cell, and E_{bulk} is the total energy of a bulk unit cell, A is the surface area of a slab unit cell. As such, a high surface energy would indicate increased reactivity with adsorbates, while low surface energy would indicate increased stability. Our calculations using Eq. (9) show that surface energies for the surface facets increase according to (001) < (100) < (110) < (111) for all the structures. This means (001) surface offer a relatively

more stable geometry, while (111) facet would likely be expected to be more reactive to impurities / adsorbates. For the clean WZ ZnO surfaces, we obtain a work function value of between 4.3 to 6.8 eV, while the corresponding literature values for ZnO surfaces vary between 3.7 and 6.0 eV [53]. Among the surface facets considered, we calculated work function values of 6.8 eV for (001), 4.5 eV for (100), 4.3 eV for (110), and 4.9 eV for (111). In view of this, we considered the (001) surface as a better suit to build-up a heterostructure of our study.

3.1. Electronic and optical properties of clean ZnO

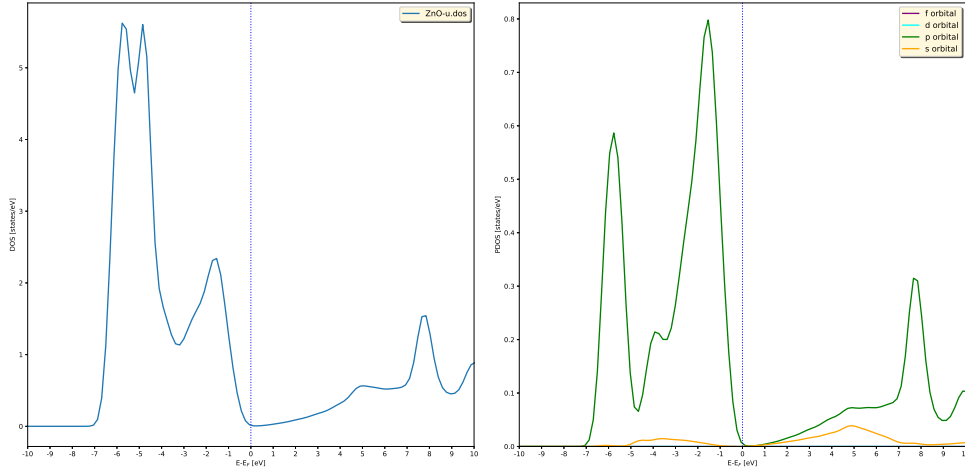


Figure 1: DOS and PDOS of bulk wurtzite ZnO.

As shown in Fig. 1, the lower part of the valence band at an energy of ~ -7 eV to ~ -4 eV shows narrow sharp peaks in DOS. The projected density of states (PDOS) is the relative contribution of a particular orbital to the DOS. As shown in Fig. 1, the p and s orbitals contribute most to the DOS curve. The p orbital has most states for occupation followed by s orbital. The p states dominate near the Fermi level, while the s states contributes in the deepest energy level.

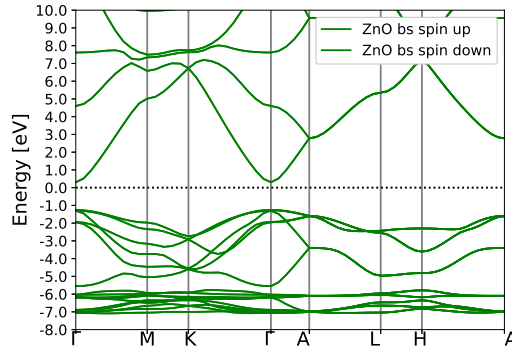


Figure 2: Band structure of bulk wurtzite ZnO.

From Fig. 2, it can be seen that the valence band maxima and conduction band minima show smaller bandgaps at identical k-points, indicating direct band. The band structure in the figure for wurtzite bulk ZnO, point $\Gamma - \Gamma$ showed the lowest energy band gap, which is ~ 3.23 eV. The excitation of electrons (from the highest valence band to the lowest conduction band) will occur at the lowest energy band gap. Thus, point $(\Gamma - \Gamma)$ is the point where electron excitation most probably occurred. The computed band gap is in agreement with the experimental value 3.37 eV.

As shown in Fig. 3, the imaginary part $\epsilon_2(\omega)$ (absorptive part) of the dielectric function (black color line) illustrates the optical transition mechanism. Each peak in the imaginary part of the dielectric function corresponds to an

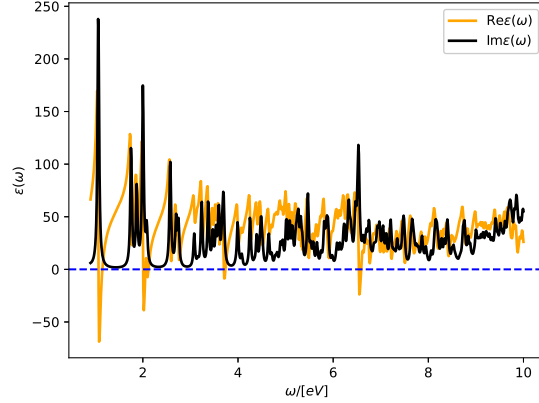


Figure 3: The real (yellow color line) and imaginary (black color line) parts of frequency-dependent complex dielectric function of wurtzite bulk ZnO with local field effects.

electronic transition. The highest peak of $\epsilon_2(\omega)$ is located at 0.61 eV, with the value of $\epsilon_2(\omega)$ is 36.69. At zero photon energy, $\epsilon_2(0)$ has a value of 10.5.

The absorption coefficient (Fig. 4) shows peaks at ranges of photon energies including at 0.6 eV, 1.2 eV, 1.8 eV, 2.1 eV, 2.5 eV, and 3.5 eV. These correspond to absorptions of near-infrared, visible, and near-ultraviolet lights. Meanwhile, the electron energy loss curve shows occurrences at photon energies exceeding 1.0 eV.

Figure 5 shows the refraction and reflectivity properties of the wurtzite ZnO. The propagation of a light beam through a translucent medium via refraction is described by the refractive index n . The static values of the index of refraction, $n(0)$, is 2.4. The reflectivity represents propagation via reflection. The static values of the reflection coefficient, $R(0)$, is 0.4.

3.2. Structural and electronic properties of graphene/ZnO heterojunction

3.2.1. Structural properties of graphene/ZnO heterojunction

We considered the adsorption of graphene on ZnO polar surfaces. The adsorption energy of graphene layer is defined by

$$E_{ads} = E_{interface} - E_{graphene} - E_{ZnO} \quad (10)$$

while,

$$e_{ads} = \frac{E_{interface} - E_{graphene} - E_{ZnO}}{n} \quad (11)$$

where e_{ads} [eV/atom] is the adsorption energy per C atom; $E_{interface}$, $E_{graphene}$, and E_{ZnO} is the total energies of the interface, graphene, and ZnO surface, respectively; n is the total number of carbon atoms in the interface. Figure 6 shows that the adsorption behaviors of the three configurations for ZnO(0001) and (000 $\bar{1}$) surfaces are almost the same.

More importantly, the long range vdW interaction plays an important role in the adsorption. Both physical and chemical adsorptions take place when graphene adheres to bare SiC [54], SiO₂ [55], and metals [56] surfaces. However, no chemical adsorption is seen when graphene adheres to ZnO surfaces. For use in photocatalysts and solar cells, the intimate but nondestructive contact between graphene and ZnO may be unique. The shortest separation distance between an atom of the adsorbed ZnO and the closest C atom of the graphene monolayer in the graphene/ZnO is 2.52 Å, which is in agreement with a literature result [57]. It looks that some sort of charge transfer from graphene layer to the underlying ZnO surface takes place at such optimum separation distance, while also the corresponding energy per atom and cohesive energies show stabilities of the structure. The geometries of interface structures of the heterojunction is given in Fig. 7, while the corresponding graphic plots of the cohesive and adsorption energies trends are given in Figs. 8 & 9, respectively. Table 2 gives quantitative values of the adsorption and cohesive energies.

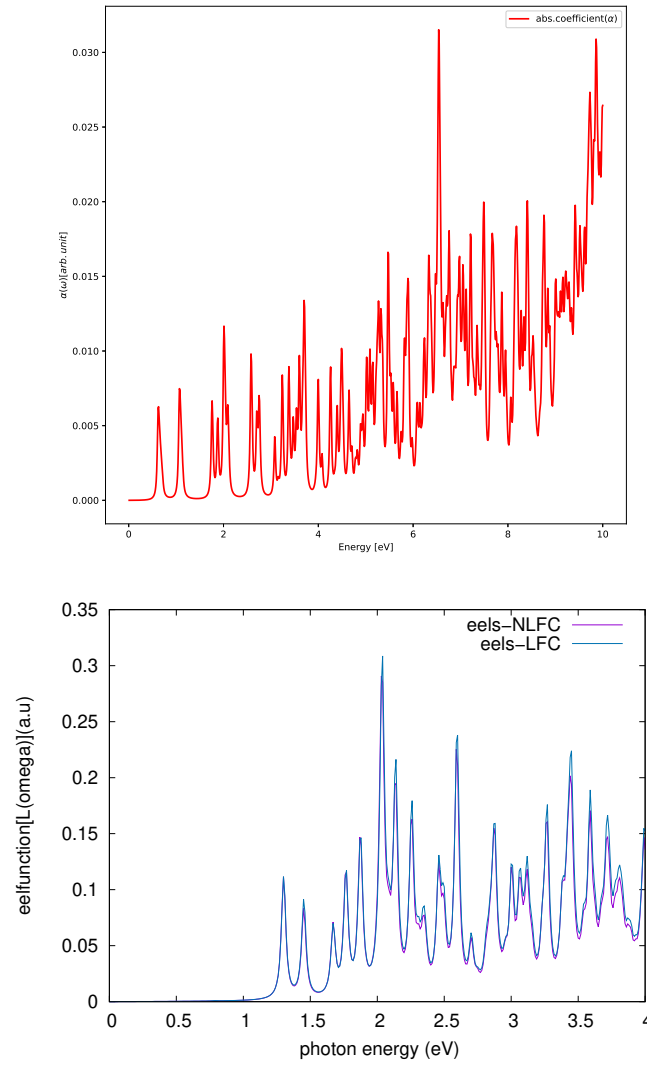


Figure 4: Absorption coefficient and electron energy loss of bulk wurtzite ZnO as a function of energy.

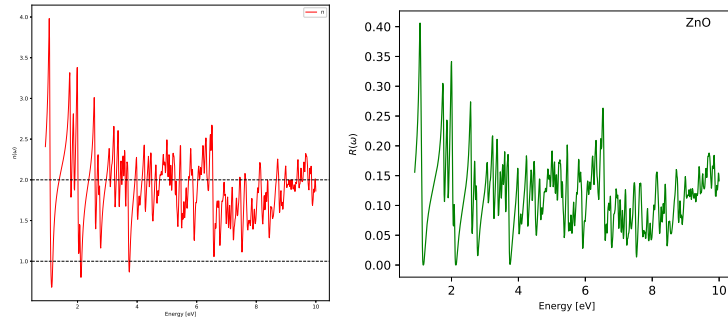


Figure 5: Index of refraction and reflectivity of bulk wurtzite ZnO as a function of energy.

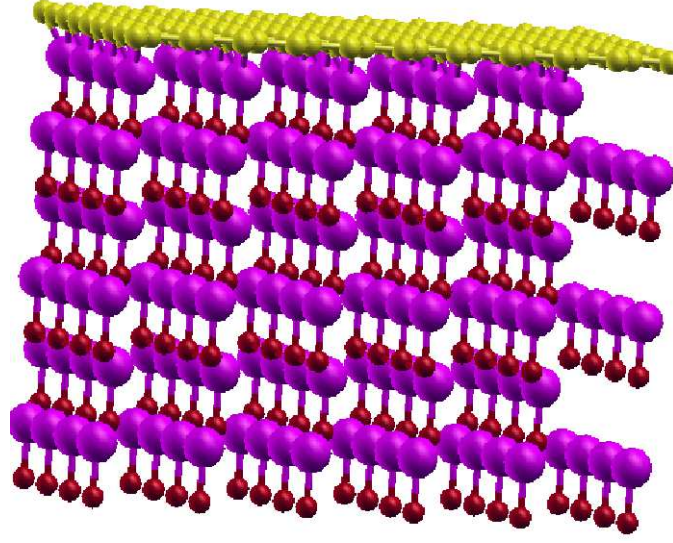


Figure 6: Graphene/ZnO heterojunction structure. Color Online. Colors: C-yellow, Zn-pink, O-red.

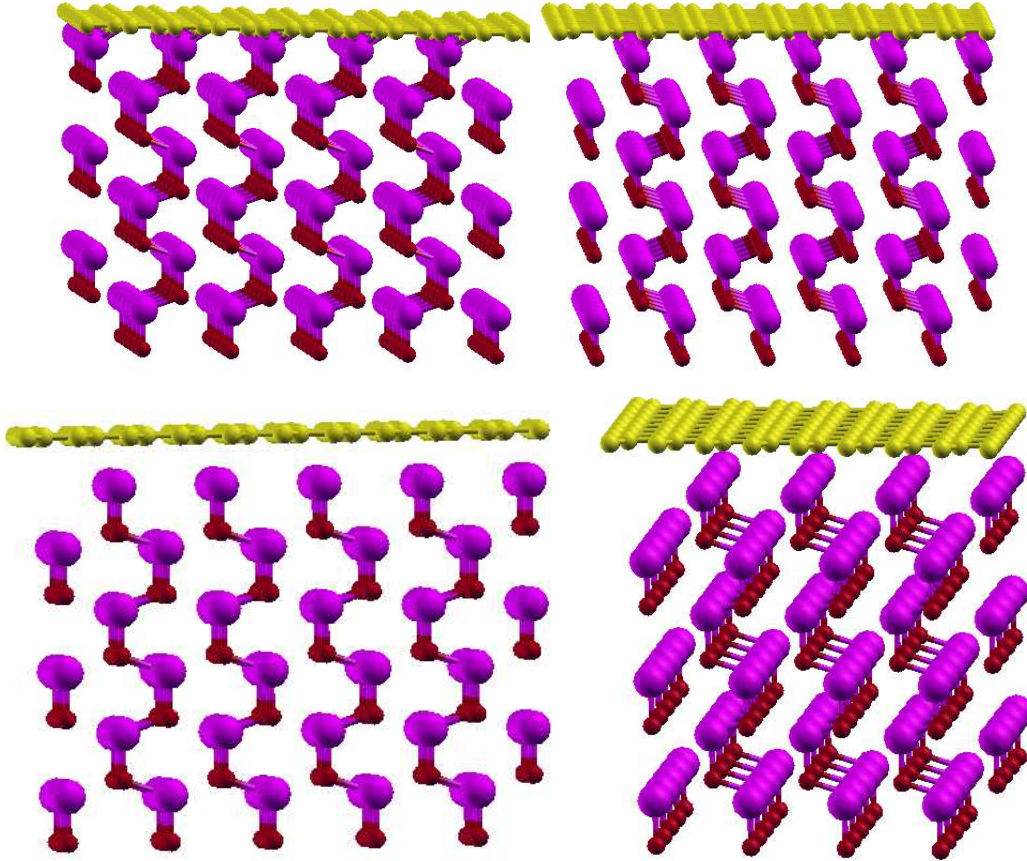


Figure 7: ZnO-001-clean-T-graphene at different equilibrium distance. Top to bottom, $d = 1.02 \text{ \AA}$, $d = 1.52 \text{ \AA}$, $d = 2.12 \text{ \AA}$, $d = 2.52 \text{ \AA}$, respectively. Color Online. Colors: C-yellow, Zn-pink, O-red.

Table 2: Adsorption energy per atom, cohesive energy, and ΔQ (charge transfer from graphene to the interface) as a function of $\frac{d_0-d}{d_0}$.

Quantity	$\frac{d_0-d}{d_0}$							
	0.99	0.79	0.59	0.39	0.27	0.00	0.15	-0.19
Energy per atom [eV]	-18.31	-14.19	-9.92	-8.60	-8.43	-8.39	-8.38	-8.36
Cohesive Energy [eV]	1.25	2.9	4.61	5.13	5.21	5.22	5.22	5.23
ΔQ [e]	+0.63	+0.19	-0.38	-0.33	-0.23	-0.13	+0.05	+0.11

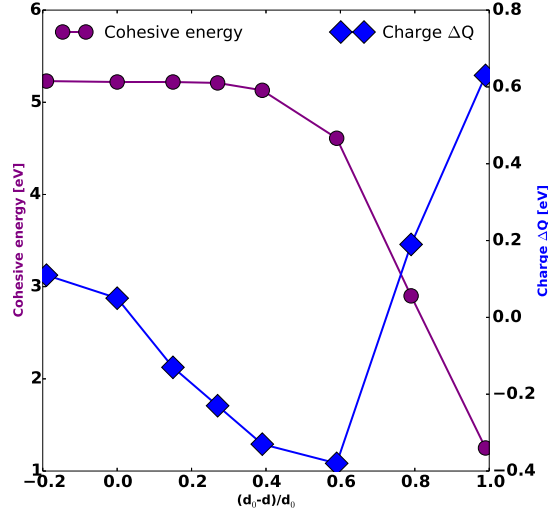


Figure 8: Cohesive energy and charge transfer ΔQ as a function of $\frac{d_0-d}{d_0}$. Color Online. Purple color: Cohesive energy, and blue color: ΔQ .

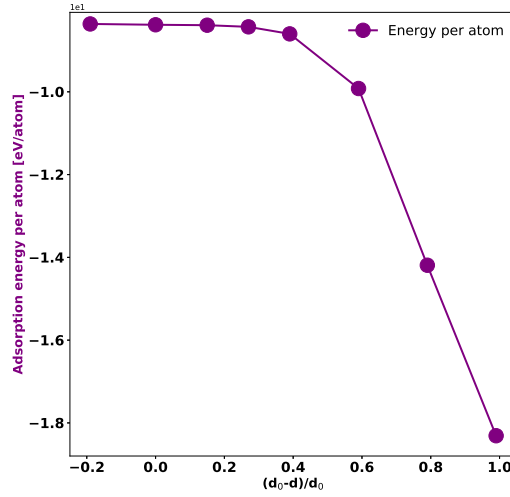


Figure 9: Adsorption energy per atom as a function of $\frac{d_0-d}{d_0}$.

3.2.2. Electronic properties of graphene/ZnO heterojunction

As shown in Fig. 10, the graphene/ZnO heterojunction shows a narrow sharp peak in the DOS at ~ 8 eV to ~ 4.5 eV which is associated with a large quantity of generated states in the valence band and nonzero DOS at the Fermi energy, indicating that graphene/ZnO has a metallic character. As PDOS is the relative contribution of a particular

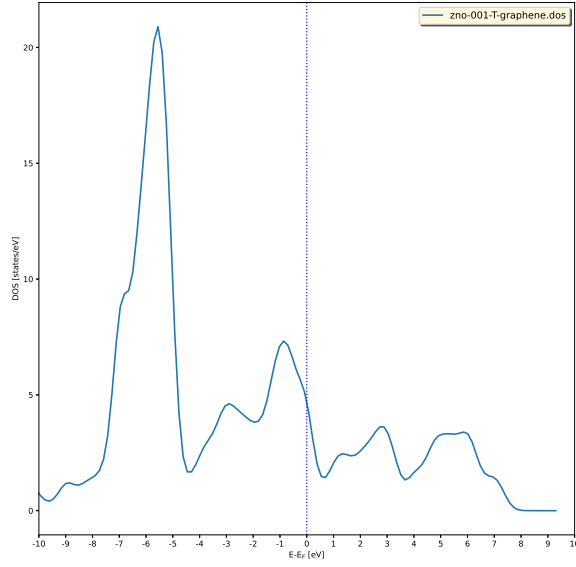


Figure 10: DOS of graphene/ZnO heterojunction.

atom/orbital to the DOS, as shown in Fig. 11, the p and s orbitals contribute to the occupation states of DOS. The p orbital has a major contribution and the s orbital has a minor contribution to the DOS in both the conduction and valence bands.

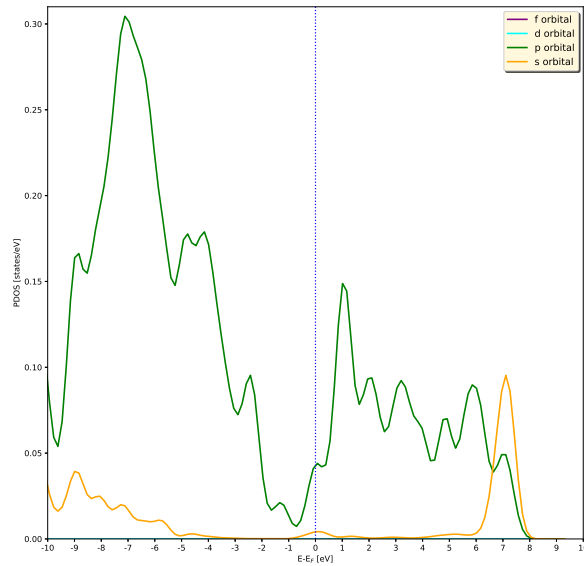


Figure 11: PDOS of graphene/ZnO heterojunction.

The charge calculations on the atoms of the unit cell shows that 0.05 electrons have been transferred from graphene atom to the Zinc Oxide. This shows that at the junction, graphene become p -type and ZnO is n -type material. A summary of the charge transfers for different layer separation distances is given in Table 2 & Fig. 8. It seems that the heterojunction increases the electrical property, (see Figs. 10 & 11), while also likely improving its optical properties. Figure 12 shows the 3D counterpart of the 2D layer interface presentations of Fig. 7. It looks from Figs. 8 & 9 that the cohesive energies and adsorption energies per atom show saturated values beginning from optimum separation

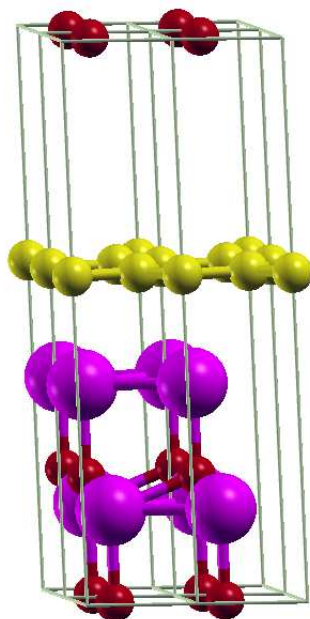


Figure 12: 3D view of heterojunction structure. Color Online. Colors: C-yellow, Zn-pink, and O-red.

distance of $d_0 = 2.52 \text{ \AA}$.

4. Conclusion

The calculation of the bulk structural, electronic and optical properties of graphene and ZnO reveals various characteristics. The structure, including equilibrium lattice constants, bulk modulus, cohesive, and formation energies are in good agreement with other experimental results. The electronic properties are studied using band gap, band structures, DOS/PDOS, and charge analysis. Surface properties of clean wurtzite ZnO polar surfaces were analysed by calculating the surface energy and work functions.

The surface energies for the surface facets increase according to $(001) < (100) < (110) < (111)$ for all the structures. Based on the outcomes, we suggest that (001) surfaces offer a relatively more stable geometries, while (111) facets would likely be expected to be more reactive to impurities/adsorbates. As a result, we have chosen the polar (001) surface to be suitable for forming the graphene/ZnO heterostructure. The electronic properties of graphene/ZnO heterostructure is revealed in bader charge, DOS, and PDOS analysis. The results show that there is a charge transfer in between graphene and ZnO and the combination/junction seems to show zero band gap. Furthermore, our findings seem to offer compelling justifications for the enhanced photocatalytic efficiency of graphene/ZnO hybrid materials.

CRediT authorship contribution statement

H.D. Etea conducted the DFT calculations, and wrote the draft manuscript, and K.N. Nigussa carried out the research process and the revised writing of the manuscript.

Declaration of Competing Interest

The authors declare that they have no known competing financial interests or personal relationships that could have appeared to influence the work reported in this paper.

Acknowledgments

We are grateful to the Ministry of Education of Ethiopia for financial support. The authors also acknowledge the Department of Physics at Addis Ababa University. The office of VPRTT of Addis Ababa University is also warmly appreciated for supporting this research under a grant number AR/053/2021.

Data Availability Statement

The data that support the findings of this study are available upon reasonable request from the authors.

References

- [1] M. Cinchetti, V. A. Dediu, L. E. Hueso, [Activating the molecular spinterface](#), *Nature Materials* 16 (2017) 507–515.
URL <https://doi.org/10.1038/nmat4902>
- [2] J. Varignon, L. Vila, A. Barthélémy, M. Bibes, [A new spin for oxide interfaces](#), *Nature Physics* 14 (2018) 322–325.
URL <https://doi.org/10.1038/s41567-018-0112-1>
- [3] S. Roche, J. Åkerman, B. Beschoten, J.-C. Charlier, M. Chshiev, S. P. Dash, B. Dlubak, J. Fabian, A. Fert, M. Guimarães, et al., [Graphene spintronics: the European Flagship perspective](#), *2D Materials* 2 (2015) 030202.
URL <https://dx.doi.org/10.1088/2053-1583/2/3/030202>
- [4] K. S. Novoselov, A. K. Geim, S. V. Morozov, D.-e. Jiang, Y. Zhang, S. V. Dubonos, I. V. Grigorieva, A. A. Firsov, [Electric field effect in atomically thin carbon films](#), *Science* 306 (2004) 666–669.
URL <https://www.science.org/doi/abs/10.1126/science.1102896>
- [5] S. Morozov, K. Novoselov, M. Katsnelson, F. Schedin, D. C. Elias, J. A. Jaszczak, A. Geim, [Giant intrinsic carrier mobilities in graphene and its bilayer](#), *Physical Review Letters* 100 (2008) 016602.
URL <https://doi.org/10.1103/PhysRevLett.100.016602>
- [6] X. Ding, H. Sun, X. Xie, H. Ren, F. Huang, M. Jiang, [Anomalous paramagnetism in graphene on hexagonal boron nitride substrates](#), *Physical Review B* 84 (2011) 174417.
URL <https://doi.org/10.1103/PhysRevB.84.174417>
- [7] A. Mattausch, O. Pankratov, [Ab initio study of graphene on SiC](#), *Physical Review Letters* 99 (2007) 076802.
URL <https://doi.org/10.1103/PhysRevLett.99.076802>
- [8] S. Bleikamp, P. J. Feibelman, T. Michely, et al., [Two-dimensional Ir cluster lattice on a graphene moiré on Ir \(111\)](#), *Physical Review Letters* 97 (2006) 215501.
URL <https://doi.org/10.1103/PhysRevLett.97.215501>
- [9] M. Z. Hossain, [Chemistry at the graphene-sio₂ interface](#), *Applied Physics Letters* 95 (2009) 143125.
URL <https://doi.org/10.1063/1.3247964>
- [10] X. Li, W. Cai, J. An, S. Kim, J. Nah, D. Yang, R. Piner, A. Velamakanni, I. Jung, E. Tutuc, et al., [Large-area synthesis of high-quality and uniform graphene films on copper foils](#), *Science* 324 (2009) 1312–1314.
URL <https://www.science.org/doi/10.1126/science.1171245>
- [11] A. Venugopal, L. Colombo, E. Vogel, [Contact resistance in few and multilayer graphene devices](#), *Applied Physics Letters* 96 (2010) 013512.
URL <https://doi.org/10.1063/1.3290248>
- [12] B. Huard, N. Stander, J. Sulpizio, D. Goldhaber-Gordon, [Evidence of the role of contacts on the observed electron-hole asymmetry in graphene](#), *Physical Review B* 78 (2008) 121402.
URL <https://doi.org/10.1103/PhysRevB.78.121402>
- [13] Ü. Özgür, Y. I. Alivov, C. Liu, A. Teke, M. Reshchikov, S. Doğan, V. Avrutin, S.-J. Cho, Morkoç, H., [A comprehensive review of ZnO materials and devices](#), *Journal of Applied Physics* 98 (2005) 11.
URL <https://doi.org/10.1063/1.1992666>
- [14] J. Zhou, N. S. Xu, Z. L. Wang, [Dissolving behavior and stability of ZnO wires in biofluids: a study on biodegradability and biocompatibility of ZnO nanostructures](#), *Advanced Materials* 18 (2006) 2432–2435.
URL <https://doi.org/10.1002/adma.200600200>
- [15] Z. Zhou, T. Komori, M. Yoshino, M. Morinaga, N. Matsunami, A. Koizumi, Y. Takeda, [Enhanced 1.54 \$\mu\$ m photoluminescence from Er-containing ZnO through nitrogen doping](#), *Applied Physics Letters* 86 (2005) 041107.
URL <https://doi.org/10.1063/1.1856692>
- [16] Z. Yin, S. Wu, X. Zhou, X. Huang, Q. Zhang, F. Boey, H. Zhang, [Electrochemical deposition of ZnO nanorods on transparent reduced graphene oxide electrodes](#), *Small* 6 (2010) 307–312.
URL <https://doi.org/10.1002/smll.200901968>
- [17] T. Kavitha, A. I. Gopalan, K.-P. Lee, S.-Y. Park, [Glucose sensing, photocatalytic and antibacterial properties of graphene–ZnO nanoparticle hybrids](#), *Carbon* 50 (2012) 2994–3000.
URL <https://doi.org/10.1016/j.carbon.2012.02.082>
- [18] W. Geng, X. Zhao, H. Liu, X. Yao, [Influence of interface structure on the properties of ZnO/graphene composites: a theoretical study by density functional theory](#), *The Journal of Physical Chemistry C* 117 (2013) 10536–10544.
URL <https://doi.org/10.1021/jp401733h>

- [19] J. Enkovaara, C. Rostgaard, J. J. Mortensen, J. Chen, M. Duřak, L. Ferrighi, J. Gavnholt, C. Glinsvad, V. Haikola, H. Hansen, et al., *Electronic structure calculations with GPAW: a real-space implementation of the projector augmented-wave method*, Journal of Physics: Condensed matter 22 (2010) 253202.
URL <https://dx.doi.org/10.1088/0953-8984/22/25/253202>
- [20] P. E. Blöchl, O. Jepsen, O. K. Andersen, *Improved tetrahedron method for Brillouin-zone integrations*, Physical Review B 49 (1994) 16223.
URL <https://doi.org/10.1103/PhysRevB.49.16223>
- [21] J. P. Perdew, K. Burke, M. Ernzerhof, *Generalized gradient approximation made simple*, Physical Review Letters 77 (1996) 3865.
URL <https://doi.org/10.1103/PhysRevLett.77.3865>
- [22] H. J. Monkhorst, J. D. Pack, *Special points for Brillouin-zone integrations*, Physical Review B 13 (1976) 5188.
URL <https://doi.org/10.1103/PhysRevB.13.5188>
- [23] G. Makov, M. Payne, *Periodic boundary conditions in ab initio calculations*, Physical Review B 51 (1995) 4014.
URL <https://doi.org/10.1103/PhysRevB.51.4014>
- [24] P. Blöchl, *Projector augmented-wave method*, Phys. Rev. B 50 (1994) 17953.
URL <https://doi.org/10.1103/PhysRevB.50.17953>
- [25] W. Kohn, L. Sham, *Self-Consistent Equations Including Exchange and Correlation Effects*, Phys. Rev. 140 (1965) A1133–A1138.
URL <https://doi.org/10.1103/PhysRev.140.A1133>
- [26] J. Enkovaara, C. Rostgaard, J. Mortensen, J. Chen, M. Duřak, L. Ferrighi, J. Gavnholt, C. Glinsvad, V. Haikola, H. Hansen, H. Kristoffersen, M. Kuisma, A. Larsen, L. Lehtovaara, M. Ljungberg, O. Lopez-Acevedo, P. Moses, J. Ojanen, T. Olsen, V. Petzold, N. Romero, J. Stausholm-Møller, M. Strange, G. Tritsaris, M. Vanin, M. Walter, B. Hammer, H. Häkkinen, G. Madsen, R. Nieminen, J. Nørskov, M. Puska, T. Rantala, J. Schiøtz, K. Thygesen, K. Jacobsen, *Electronic structure calculations with GPAW: a real-space implementation of the projector augmented-wave method*, J. Phys.: Condens. Matter 22 (2010) 253202.
URL <https://doi.org/10.1088/0953-8984/22/25/253202>
- [27] J. Mortensen, L. Hansen, K. Jacobsen, *Real-space grid implementation of the projector augmented wave method*, Phys. Rev. B 71 (2005) 035109.
URL <https://doi.org/10.1103/PhysRevB.71.035109>
- [28] H. Schlegel, *Optimization of equilibrium geometries and transition structures*, J. Comp. Chem. 3 (1982) 214.
URL <https://doi.org/10.1002/jcc.540030212>
- [29] P. Feynman, *Forces in Molecules*, Phys. Rev. 56 (1939) 340.
URL <https://doi.org/10.1103/PhysRev.56.340>
- [30] O. Nielsen, R. Martin, *Quantum-mechanical theory of stress and force*, Phys. Rev. B 32 (1985) 3780.
URL <https://doi.org/10.1103/PhysRevB.32.3780>
- [31] R. Wentzcovitch, J. Martins, *First principles molecular dynamics of Li: Test of a new algorithm*, Solid State Commun. 78 (1991) 831.
URL [https://doi.org/10.1016/0038-1098\(91\)90629-A](https://doi.org/10.1016/0038-1098(91)90629-A)
- [32] J. Perdew, K. Burke, M. Ernzerhof, *Generalized Gradient Approximation Made Simple*, Phys. Rev. Lett. 77 (1996) 3865.
URL <https://doi.org/10.1103/PhysRevLett.77.3865>
- [33] A. Liechtenstein, V. Anisimov, J. Zaanen, *Density-functional theory and strong interactions: Orbital ordering in mott-hubbard insulators*, Phys. Rev. B 52 (1995) R5467.
URL <https://doi.org/10.1103/PhysRevB.52.R5467>
- [34] S. Dudarev, G. Botton, S. Savrasov, C. Humphreys, A. Sutton, *Electron-energy-loss spectra and the structural stability of nickel oxide: an LSDA+U study*, Phys. Rev. B 57 (1998) 1505.
URL <https://doi.org/10.1103/PhysRevB.57.1505>
- [35] F. Murnaghan, *The Compressibility of Media under Extreme Pressures*, Proc. Natl. Acad. Sci. 30 (1944) 244.
URL <https://doi.org/10.1073/pnas.30.9.244>
- [36] S. Awulachew, K. Nigussa, *First principles study of adsorption and simulation of desorption properties of Pd_{1-x}Ag_x surface alloy*, Computational Condensed Matter 33 (2022) e00741.
URL <https://doi.org/10.1016/j.cocom.2022.e00741>
- [37] S. Grimme, *Semiempirical GGA-type density functional constructed with a long-range dispersion correction*, Journal of Computational Chemistry 27 (2006) 1787–1799.
URL <https://doi.org/10.1002/jcc.20495>
- [38] T. Jayasekera, S. Xu, K. W. Kim, M. B. Nardelli, *Electronic properties of the graphene/6H-SiC (000 $\bar{1}$) interface: A first-principles study*, Physical Review B 84 (2011) 035442.
URL <https://doi.org/10.1103/PhysRevB.84.035442>
- [39] M. Vanin, J. J. Mortensen, A. Kelkkanen, J. M. Garcia-Lastra, K. S. Thygesen, K. W. Jacobsen, *Graphene on metals: A van der Waals density functional study*, Physical Review B 81 (2010) 081408.
URL <https://doi.org/10.1103/PhysRevB.81.081408>
- [40] M. Dion, H. Rydberg, E. Schröder, D. C. Langreth, B. I. Lundqvist, *Van der waals density functional for general geometries*, Physical Review Letters 92 (2004) 246401.
URL <https://doi.org/10.1103/PhysRevLett.92.246401>
- [41] R. Haumont, I. A. Kornev, S. Lisenkov, L. Bellaiche, J. Kreisler, B. Dkhil, *Phase stability and structural temperature dependence in powdered multiferroic BiFeO₃*, Physical Review B 78 (2008) 134108.
URL <https://link.aps.org/doi/10.1103/PhysRevB.78.134108>
- [42] T. Ada, K. Nigussa, L. Deja, *Impact of a dopant vis-a-vis site and concentration on the photovoltaic effect of BiFeO₃*, Physica B: Condensed Matter 647 (2022) 414366.
URL <https://doi.org/10.1016/j.physb.2022.414366>

- [43] M. Hybertsen, S. Louie, *Ab initio* static dielectric matrices from the density-functional approach: Formulation and application to semiconductors and insulators, Phys. Rev. B 35 (1987) 5585.
URL <https://doi.org/10.1103/PhysRevB.35.5585>
- [44] M. Gajdoš, K. Hummer, G. Kresse, J. Furthmüller, F. Bechstedt, Linear optical properties in the projector-augmented wave methodology, Phys. Rev. B 73 (2006) 045112.
URL <https://doi.org/10.1103/PhysRevB.73.045112>
- [45] M. Shishkin, G. Kresse, Implementation and performance of the frequency-dependent GW method within the PAW framework, Phys. Rev. B 74 (2006) 035101.
URL <https://doi.org/10.1103/PhysRevB.74.035101>
- [46] F. Wooten, Optical Properties of Solids, Academic Press, New York, 1972.
- [47] T. Ada, K. Nigussa, L. Deja, The effect of non-centrosymmetry on optical and electronic properties of BaHfO₃ perovskite, Computational Condensed Matter 26 (2021) e00524.
URL <https://doi.org/10.1016/j.cocom.2020.e00524>
- [48] T. Shen, C. Hu, H. L. Dai, W. L. Yang, H. C. Liu, X. L. Wei, First principles study of structural, electronic and optical properties of BiFeO₃ in ferroelectric and par Materials Research Innovations 19 (2015) S5–684–S5–688.
URL <https://doi.org/10.1179/1432891714Z.0000000001176>
- [49] Z. Teng, J. Jiang, G. Chen, C. Ma, F. Zhang, The electronic structures and optical properties of B, C or N doped BaTiO₃, AIP Advances 8 (2018) 095216.
URL <https://doi.org/10.1063/1.5047094>
- [50] R. Weast, CRC Handbook of Chemistry and Physics, CRC Press, Boca Raton, FL, 1997.
- [51] S. Desgreniers, High-density phases of ZnO: Structural and compressive parameters, Physical Review B 58 (1998) 14102.
URL <https://doi.org/10.1103/PhysRevB.58.14102>
- [52] M. Rajalakshmi, A. K. Arora, Stability of Monoclinic Selenium Nanoparticles, Solid State Physics 44 (2002) 109.
- [53] K. Jacobi, G. Zwicker, A. Gutmann, Work function, electron affinity and band bending of zinc oxide surfaces, Surface Science 141 (1984) 109–125.
URL [https://doi.org/10.1016/0039-6028\(84\)90199-7](https://doi.org/10.1016/0039-6028(84)90199-7)
- [54] T. Jayasekera, S. Xu, K. W. Kim, M. B. Nardelli, Electronic properties of the graphene/6H-SiC (000 $\bar{1}$) interface: A first-principles study, Physical Review B 84 (2011) 035442.
URL <https://doi.org/10.1103/PhysRevB.84.035442>
- [55] X. Fan, W. Zheng, V. Chihaiia, Z. Shen, J.-L. Kuo, Interaction between graphene and the surface of SiO₂, Journal of Physics: Condensed Matter 24 (2012) 305004.
URL <https://dx.doi.org/10.1088/0953-8984/24/30/305004>
- [56] C. Gong, G. Lee, B. Shan, E. M. Vogel, R. M. Wallace, K. Cho, First-principles study of metal–graphene interfaces, Journal of Applied Physics 108 (2010) 123711.
URL <https://doi.org/10.1063/1.3524232>
- [57] B. Das, B. Choudhury, A. Gomathi, A. K. Manna, S. Pati, C. Rao, Interaction of inorganic nanoparticles with graphene, ChemPhysChem 12 (2011) 937–943.
URL <https://doi.org/10.1002/cphc.201001090>